ACS APPLIED NANO MATERIALS

www.acsanm.org Article

# Palladium Nanoparticles on Covalent Organic Framework Supports as Catalysts for Suzuki–Miyaura Cross-Coupling Reactions

Jianguo Liu,*,‖ Hao Zhan,‖ Nan Wang,‖ Yanpei Song, Chenguang Wang, Xinming Wang, Longlong Ma,* and Lungang Chen

Cite This: *ACS Appl. Nano Mater.* 2021, 4, 6239–6249 Read Online

ACCESS | Metrics & More | Article Recommendations | Supporting Information

**ABSTRACT:** Suzuki–Miyaura cross-coupling (SMC) reaction by palladium (Pd) catalysis is widely used in cross-coupling chemistry synthesis for C—C bond formation, yet the biaryl products are generally lacking halo substituents due to highly active palladium species. Suitable catalysts according to this property for the region-selective SMC synthesis of biaryl derivatives with halo substituents did not receive due and sufficient attention. Here, we report the facile synthesis of a covalent organic frameworks (COFs)-supported nanoparticles Pd catalyst that can region-selectively catalyze the SMC reaction of aryl boronic acids and aryl halides, especially with halogenated aryl boronic acids. The methodology exhibits mild operating conditions, broad functional group tolerance, and environmental friendliness and can be strategically applied for cross-coupling scenarios governed by sequential transition metal catalysts to build with or without a halo-substituted moiety. The Pd/COF-SMC nanoparticles catalysts are stable and reusable and succeed in synthesizing halo-substituted biaryl products in excellent yield, which avoids the homocoupling of halogenated aryl boronic acid. The most outstanding advantage is the precise regulation of nanoparticles Pd activity with the well-designed COF ligand.

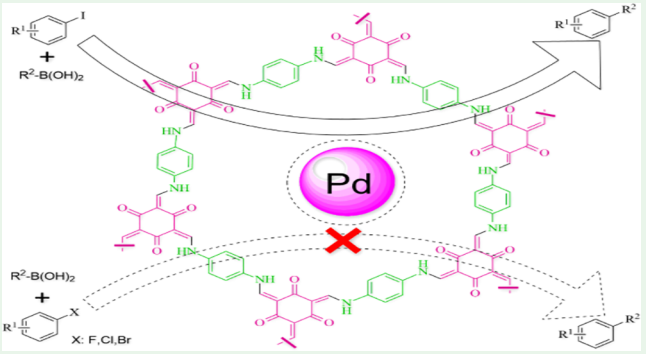


**KEYWORDS:** *covalent organic framework, precise regulation, palladium catalysis, Suzuki–Miyaura cross-coupling reaction, halo-substituted biaryl compounds*

## 1. INTRODUCTION

Cross-coupling reactions such as Heck, Negishi, Stille, Kumada, Sonogashira, Suzuki–Miyaura, etc. have been exploited and applied extensively in synthetic organic chemistry due to their excellent capacity for constructing new carbon–carbon bonds.[1,2] Among them, the Suzuki–Miyaura cross-coupling (SMC) of aryl boronic acids/esters and aryl halides is a promising and powerful approach toward the construction of biaryl derivatives that are found in the building blocks of many pharmaceuticals, agrochemicals, polymers, and natural products.[3−6] In general, the SMC reaction is quite often performed in the presence of palladium (Pd) catalysts, exhibiting multiple advantages of excellent catalytic activity, mild operating conditions, and broad functional group tolerance.[7] Since the first report of the Pd-catalyzed SMC reaction in 1979,[8] academic research and industrial applications focusing on this reaction have increased exponentially over the past decades, as affirmed by the award of the 2010 Nobel Prize in chemistry.[2] Accordingly, thousands of Pd catalysts with various ligand systems have been gradually developed to revolutionize this field. Homogenous categories are primarily exploited and widely employed, including phosphane-based ligands such as tertiary-, hemilable-, biophenyl-, and indole-types[9,10] and nitrogen-containing ligands like N-heterocyclic carbenes, amines, oximes, and Schiff bases.[11−14] Although this kind of catalyst is usually highly active, a major problem is the difficulty in their recovery and recycling. By comparison, many novel heterogeneous nanoparticles Pd catalysts have been designed in recent years by immobilizing Pd complexes on various supports like mesoporous silica,[15] zeolites,[16] carbon,[17] and metal–organic frameworks (MOFs).[18,19] The use of these catalysts facilitates the SMC chemistry process and achieves the efficient utilization of the increasingly expensive Pd metal. However, there would be still some obvious drawbacks for them including leaching, agglomeration, and deactivation.[20] Thus, it is a need to seek more suitable nanoscale supports to disperse, stabilize, and recycle Pd nanoparticles. Most importantly, due to the uncontrolled selectivity of active Pd toward aryl halides, the homocoupling of aryl halide or aryl boronic halo-substituent

Received: April 16, 2021
Accepted: June 2, 2021
Published: June 13, 2021

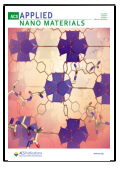






https://doi.org/10.1021/acsanm.1c01038
*ACS Appl. Nano Mater.* 2021, 4, 6239–6249

**Scheme 1. (a) Preliminary Verification of Hypothesis: Precise Regulation of Palladium Activity with Covalent Organic Framework (COF) and (b) Comparison of Pd/COF-SMC$_2$ and Other Highly Active Pd Catalyst**

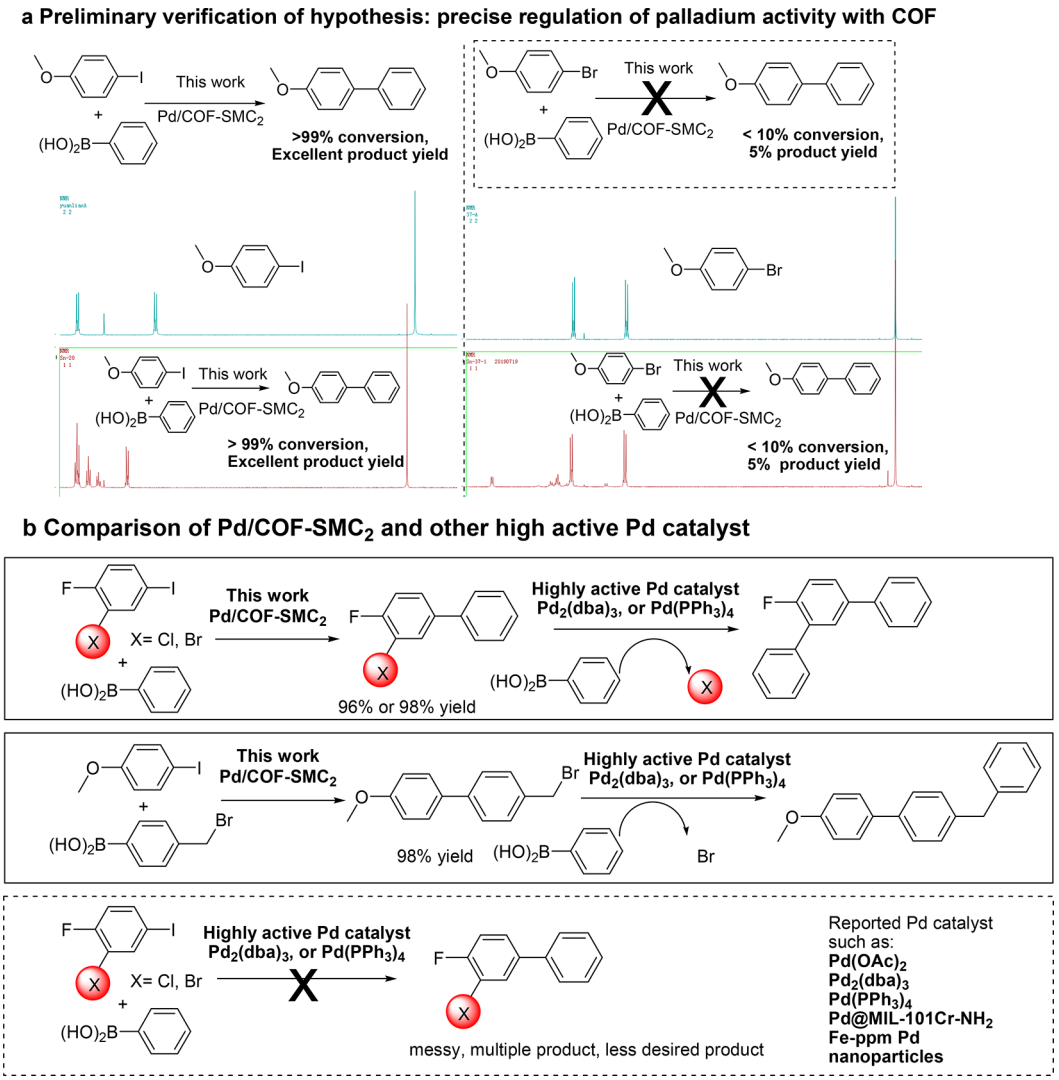


accompanied the reaction that resulted in the low yield of the halo-substituted biaryl products. It is a fact and also an issue that biaryl derivatives produced from the current Pd-catalyzed SMC reaction generally lacked halo substituents (the target halo-substituted product normally with a low yield due to self-coupling of the reagent itself) since highly active transition metal species no matter homogeneous or heterogeneous catalysts were employed as showed in Scheme S1a.

To date, several works of literature focusing on the application of covalent organic framework (COF)-supported nanoparticles Pd catalysts in SMC reaction have been reported,[35−38] displaying a promising option for catalyzing the SMC reaction efficiently. However, in the previously reported synthesis methods, the SMC reaction products are predominately nonhalo-substituted. Since halo-hydrocarbons are an essential type of organic compounds that present in and applied as synthetic intermediates of biologically active compounds and natural products. Even though the general reactivity order of aryl halides R-Cl ≪ R-Br ∼ R-OTf < R-I has been well-recognized,[21,22] designing suitable catalysts according to this property for the region-selective SMC synthesis of biaryl derivatives with halo substituents did not receive due and sufficient attention. N,N-Ligands have been reported and used exclusively for controlling the activity of the transition metal catalyst.[7,23−34] Herein, in this work, we proposed to design and synthesize the nanoparticles Pd-COF catalyst, which regulated the selectivity of active Pd species via electron-donating N,N-ligand. The target Pd-COF nanoparticles catalyst selectively catalyzed phenylboronic acid with aryl iodide in excellent product yield instead of aryl bromide during the SMC process (Scheme 1a), which successfully verified the hypothesis on the precise regulation of Pd activity with a COF structure. Hence, under the controllable activity of catalyzed Pd-COF, the homocoupling of halogenated aryl boronic acid should be avoided and the halo-substituted biaryl products would be obtained in high yield as showed in Scheme S1b. This was then verified by the comparison of using nanoparticles Pd/COF-SMC$_2$ from our work and other highly active Pd catalysts (Scheme 1b). Under the optimized reaction conditions in this work using Pd/COF-SMC$_2$, an excellent yield of halo-substituted biaryl products was obtained starting from aryl halides with aryl boronic acids/halogenated aryl boronic acids, which could be used as q starting martial for further Suzuki coupling using a highly active Pd catalyst. As for the comparison, using the highly active Pd catalyst, the aryl halides with aryl boronic acids/halogenated aryl boronic acids gave a reaction


https://doi.org/10.1021/acsanm.1c01038
ACS Appl. Nano Mater. 2021, 4, 6239−6249

**Table 1. Optimization of SMC Reaction**

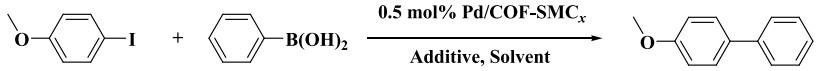


| entry[a] | catalyst | additive | solvent | temperature (°C) | time (h) | concentration (%)[b] |
|---|---|---|---|---|---|---|
| 1 | Pd/COF-SMC$_1$ | $K_2CO_3$ | xylene | 150 | 3 | 41 |
| 2 | Pd/COF-SMC$_2$ | $K_2CO_3$ | xylene | 150 | 3 | 47 |
| 3 | Pd/COF-SMC$_3$ | $K_2CO_3$ | xylene | 150 | 3 | 44 |
| 4 | Pd/COF-SMC$_4$ | $K_2CO_3$ | xylene | 150 | 3 | 11 |
| 5 | Pd/COF-SMC$_2$ | $K_2CO_3$ | EtOH | 80 | 3 | 99 |
| 6 | Pd/COF-SMC$_2$ | $K_2CO_3$ | Toluene | 120 | 3 | 24 |
| 7 | Pd/COF-SMC$_2$ | $K_2CO_3$ | DCM | 50 | 3 | 13 |
| 8 | Pd/COF-SMC$_2$ | $K_2CO_3$ | THF | 70 | 3 | 26 |
| 9 | Pd/COF-SMC$_2$ | $K_2CO_3$ | EtOAc | 80 | 3 | 28 |
| 10 | Pd/COF-SMC$_2$ | $K_2CO_3$ | EtOH/$H_2O$ | 80 | 3 | 95 |
| 11 | Pd/COF-SMC$_2$ | $K_2CO_3$ | THF/$H_2O$ | 100 | 3 | 93 |
| 12 | Pd/COF-SMC$_2$ | $K_2CO_3$ | i-PrOH | 90 | 3 | 51 |
| 13 | Pd/COF-SMC$_2$ | $K_2CO_3$ | MeOH | 100 | 3 | 92 |
| 14 | Pd/COF-SMC$_2$ | $K_2CO_3$ | Acetone | 60 | 3 | 14 |
| 15 | Pd/COF-SMC$_2$ | $Na_2CO_3$ | EtOH | 80 | 3 | 41 |
| 16 | Pd/COF-SMC$_2$ | NaOH | EtOH | 80 | 3 | 98 |
| 17 | Pd/COF-SMC$_2$ | $Cs_2CO_3$ | EtOH | 80 | 3 | 99 |
| 18 | Pd/COF-SMC$_2$ | KoH | EtOH | 80 | 3 | 99 |
| 19 | Pd/COF-SMC$_2$ | $CaCO_3$ | EtOH | 80 | 3 | 99 |
| 20 | Pd/COF-SMC$_2$ | $Cs_2CO_3$ | EtOH | 80 | 1 | 99 |
| 21[c] | Pd/COF-SMC$_2$ | $Cs_2CO_3$ | EtOH | 80 | 3 | 99 |
| 22[d] | Pd/COF-SMC$_2$ | $Cs_2CO_3$ | EtOH | 80 | 3 | 98 |

[a]Unless otherwise stated, the reaction conditions are 0.5 mmol of 1-iodo-4-methoxybenzene, 0.75 mmol of phenylboronic acid, 1.0 mmol of additive, 0.5 mol % of Pd/COF-SMC$_x$, and 4 mL of solvent. [b]Determined by $^1$H NMR spectroscopy, based on aryl halide. [c]0.75 mmol of $Cs_2CO_3$ was used. [d]0.6 mmol of $Cs_2CO_3$ was used.

mixture and a less desired product as well as a difficult purification.

Herein, we examined the representative Pd-catalyzed SMC reaction using our heterogeneous Pd/COF-SMC$_x$ catalysts. As listed in Table 1, a series of heterogeneous COF-based Pd catalysts, Pd/COF-SMC$_1$, Pd/COF-SMC$_2$, Pd/COF-SMC$_3$, and Pd/COF-SMC$_4$, were employed to make a comparison of this reaction in xylene solvent under previously reported standard reaction conditions.[35] Unlike the previous reported COF-supported catalyst, our prepared catalyst Pd/COF-SMC$_x$ showed low reactivity under the same reaction conditions. This finding could be due to the fact that the stronger coordination between COF ligand and $Pd(OAc)_2$ would result in lower catalytic reactivity. In other content, we hypothesized that the precise control of Pd activity by COF ligand affection could avoid homocoupling problems, which has been a great challenge in the previous highly active homogeneous Pd catalyst without selectivity for halo Cl-, Br-, and I-substituted substrates. The solvent had a great effect on this Pd/COF-SMC$_2$-catalyzed SMC reaction. Surprisingly, Pd/COF-SMC$_2$ possesses the best performance by employing alcoholic solvent EtOH. Stronger base $Cs_2CO_3$ has the best catalytic performance under the base evaluation. Amazingly, this SMC reaction could also perform in a short reaction time without losing significant product yield (entry 20) using the prepared Pd/COF-SMC$_2$ catalyst.

Herein, we synthesize a series of Pd-supported COFs nanoparticles catalysts (defined as Pd/COF-SMC$_x$) and probe their catalytic capabilities toward the region-selective SMC reactions of aryl boronic acids and aryl halides, especially with halogenated aryl boronic acids. The phase structure, chemical composition, and morphology of the COF carrier and Pd/COF catalyst were characterized. Meanwhile, the relevant SMC reactions were sequentially studied in detail. First, on the basis of the conventional aryl halide and phenylboronic acid, the conditions for the SMC reaction including the catalyst, the additive, the solvent, the temperature, and the time were optimized. Then, under an optimal condition, various aryl boronic acids and aryl halides were employed to verify the catalytic activity. Because of the ideal strong coordination between active Pd (II) species and COF material, the optimal Pd/COF-SMC$_2$ presents good catalytic performance for the region-selective SMC reaction. In comparison to other previous reported work,[5,35,37] a less hazardous solvent and mild operating conditions have been achieved. The most outstanding advantage of this method is undoubtedly characterized as the precise regulation of active Pd species. Using this facile synthesis of the Pd/COF-SMC$_2$ catalyst, we undertook the synthesis of >40 biaryl products, and more than 20 halo-substituted biaryl products were obtained in excellent yield that avoids the self-coupling of halogenated aryl boronic acid, just like in our proposed design route (Scheme S2c). Furthermore, the catalyst can be recycled three times without a significant decrease of catalytic activity.

## 2. EXPERIMENTAL SECTION

**2.1. Materials.** All chemicals, unless otherwise noted, were purchased without any further purification. All reactions were conducted in glass ampules with magnetic stirring under a dry nitrogen atmosphere, which was ensured using a Schlenk line. The solvents EtOH (≥99.5%, anhydrous grade), $CH_2Cl_2$ (≥99.9%, GC), DMF (≥99.9%, BR), xylene (≥99.9%, anhydrous grade), toluene (≥99.5%, AR), THF (≥99.0%, AR), EtOAc (≥99.5%, AR), i-PrOH (≥99.5%, AR), MeOH (≥99.9%, GC), and acetone (≥99.5%, AR) were selected and used directly in this work.



https://doi.org/10.1021/acsanm.1c01038
ACS Appl. Nano Mater. 2021, 4, 6239−6249

**Scheme 2. Preparation of COF-SMC$_x$ and Pd/COF-SMC$_x$**

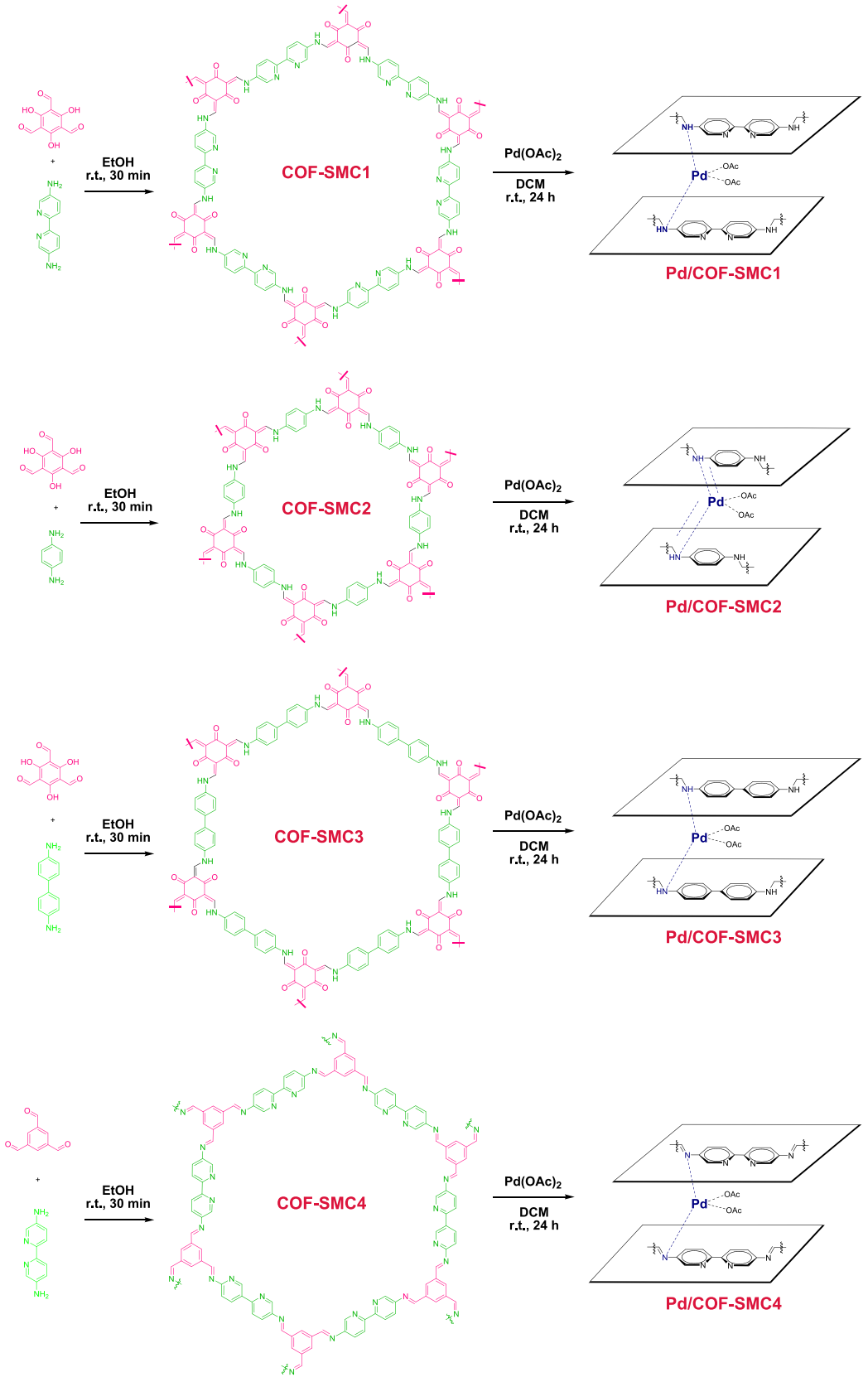


**2.2. Synthesis of COF-SMC$_x$.** The COF-SMC$_2$ was synthesized by reacting 1,3,5-triformylphloroglucinol (2.38 mmol) and *p*-phenylenediamine (3.57 mmol) at room temperature for 30 min in the presence of solvent EtOH (60 mL). The reaction products were collected and then dispersed with solvent DMF at 160 °C for 4 h. After being isolated by filtration, the resultant solid product was immersed in solvent EtOH at 80 °C for 2 h. Finally, the powder material was obtained by refiltration and vacuum drying at 80 °C for 24 h. To have a



https://doi.org/10.1021/acsanm.1c01038
*ACS Appl. Nano Mater.* 2021, 4, 6239−6249

better comparison, COF-SMC$_1$, and COF-SMC$_3$ were synthesized following the same procedure by replacing *p*-phenylenediamine with 2,2′-bipyridine-5,5′-diamine and 4,4′-diaminobiphenyl, respectively. COF-SMC$_4$ was synthesized using the same method based on another aldehyde feedstock (benzene-1,3,5-tricarbaldehyde) and 2,2′-bipyridine-5,5′-diamine. The detailed information is shown in Scheme 2.

**2.3. Synthesis of Pd/COF-SMC$_x$.** Presynthesized COF-SMC$_x$ (165 mg) and Pd(OAc)$_2$ (20 mg) were immersed in the solvent $CH_2Cl_2$ (10 mL), and the mixture was stirred at room temperature for 24 h to complete the load of the active Pd component. After that, the resultant residue was recovered by suction filtration and then eluted with the above solvent ($CH_2Cl_2$) for 24 h. At last, the target heterogeneous catalyst sample of Pd/COF-SMC$_x$ was acquired by the vacuum drying of the solid residue at 80 °C for 12 h.

**2.4. Characterizations.** The reaction product was purified by column chromatographic separations using Kiesel gel 60 H silica gel (particle size: 0.063−0.100 mm) or Brockmann I, activated, basic $Al_2O_3$ (particle size: ∼150 mesh). The reaction was monitored by thin-layer chromatography (TLC) on aluminum plates coated with Kieselgel 60 (0.20 mm, UV254) and visualized under ultraviolet light ($\nu$ = 254 nm). $^1$H and $^{13}$C NMR spectra of liquid products were recorded on an AVANCE III HD-400 NMR spectrometer (Bruker) using $CDCl_3$ solvent, which was referenced to the residual (7.26 ppm) and central (77.0 ppm) peaks of $CDCl_3$. Several analytical techniques (X-ray powder diffraction (XRD), X-ray photoelectron spectroscopy (XPS), Fourier-transform infrared spectroscopy (FTIR), scanning electron microscopy (SEM), transmission electron microscopy (TEM), and nitrogen adsorption isotherms) were used to characterize the structures of solid materials (catalyst and carrier). XRD powder patterns were performed on an X'Pert Pro diffractometer (PANalytical) employing Cu K$\alpha$ radiation ($\lambda$ = 0.15406 nm) at an operating current of 40 mA and a voltage of 40 kV. The scan was adjusted from 2.5° to 50° in 2$\theta$ range with 2 s/step counter-times and 0.0167° step size. XPS spectra (C 1s, N 1s, O 1s, and Pd 3d) were recorded by an ESCALAB 250Xi XPS spectrometer (Thermo VG Scientific) operating at a monochromatic Al K$\alpha$ X-ray source (150 W, 1486.68 eV) with a 30 eV pass energy, a 0.1 eV step size, a 500 $\mu$m spot size in diameter, and a 90° electron takeoff angle. All spectra were evaluated using Advantage software on the basis of the following principles: (1) the binding energy calibration using principal C 1s peak (284.6 eV); (2) the peak fitting using a fwhm of 0.50−2.50 eV, a Gaussian−Lorentzian function of 30%, and a background subtraction of Smart-type; (3) the curve resolution using specific type and binding energy for palladium, carbon, nitrogen, and oxygen structures, as follows, (3.1) Pd 3d, Pd(II) (338.1 ± 0.3 eV, 343.3 ± 0.3 eV) and Pd(0) (335.8 ± 0.3 eV, 341.0 ± 0.3 eV); (3.2) C 1s, C—H/C—C/ C=C (284.6 ± 0.2 eV), C—(O, N) (286.1 ± 0.3 eV), and O=C—(C, OH) (288.5 ± 0.5 eV); (3.3) N 1s, amine-N (399.9 ± 0.3 eV), pyrrolic-N (400.4 ± 0.2 eV), and pyridinic-N (398.8 ± 0.2 eV); (3.4) O 1s, O=C (531.4 ± 0.3 eV), C—O—(C, H) (532.5 ± 0.5 eV), and C—O—OH (535.2 ± 0.3 eV). FTIR spectra were measured on a Tensor 27 FTIR spectrometer (Bruker) in absorbance mode with the range 4000−400 cm$^{-1}$ (resolution: 4 cm$^{-1}$) using KBr as the reference. The morphologies were recognized using a Hitachi SU-70 FESEM (Hitachi) operating at 10 kV and a JEM-2100F HRTEM (JEOL) operating at 200 kV. Nitrogen adsorption isotherms were measured by a ASIQMO002−2 apparatus (Quantachrome) at liquid nitrogen temperature after their vacuum degassing at 120 °C for 10 h. The Brunauer−Emmett−Teller (BET) method was selected to calculate the specific surface area.

**2.5. Evaluation of Catalyst Activity.** To evaluate the catalyst activity of Pd/COF-SMC$_x$, the typical procedure run of SMC reaction in relation to Pd/COF-SMC$_2$ was as follows: the catalyst Pd/COF-SMC$_2$ (3 mg), the aryl halide (0.5 mmol), the aryl boronic acid (0.75 mmol), the alkalic additive $Cs_2CO_3$ (325.8 mg, 1.0 mmol), and the solvent EtOH (4 mL) were introduced into the reactor, which was operated at 80 °C under a $N_2$ atmosphere in a stirring and refluxing mode. TIC analysis was employed to monitor the reaction process. After the completion of the reaction, the solid catalyst was recovered by two sequential steps: the centrifugal separation of the mixture and the triple-wash of the solid with $CH_2Cl_2$ (5 mL). The desired liquid organic product was obtained following three procedures: (1) the wash of liquid phase using deionized water (20 mL) to remove the alkalic additive; (2) the vacuum evaporation of liquid phase to obtain the crude organics; and (3) the further purification of the crude organics by the silica gel column chromatography method.

## 3. RESULTS AND DISCUSSION

The PXRD profile and FTIR spectra of COF material carrier COF-SMC$_2$ and its corresponding catalyst Pd/COF-SMC$_2$ are

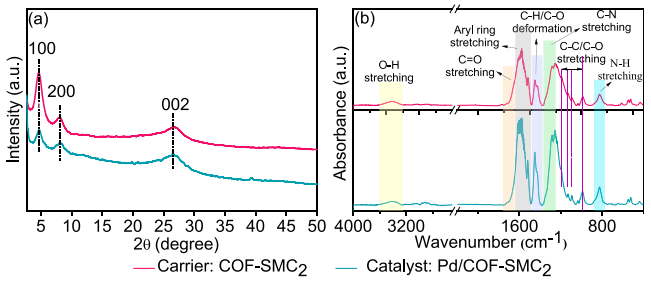


**Figure 1.** Experimental (a) PXRD and (b) FTIR analyses of the target catalyst and carrier.

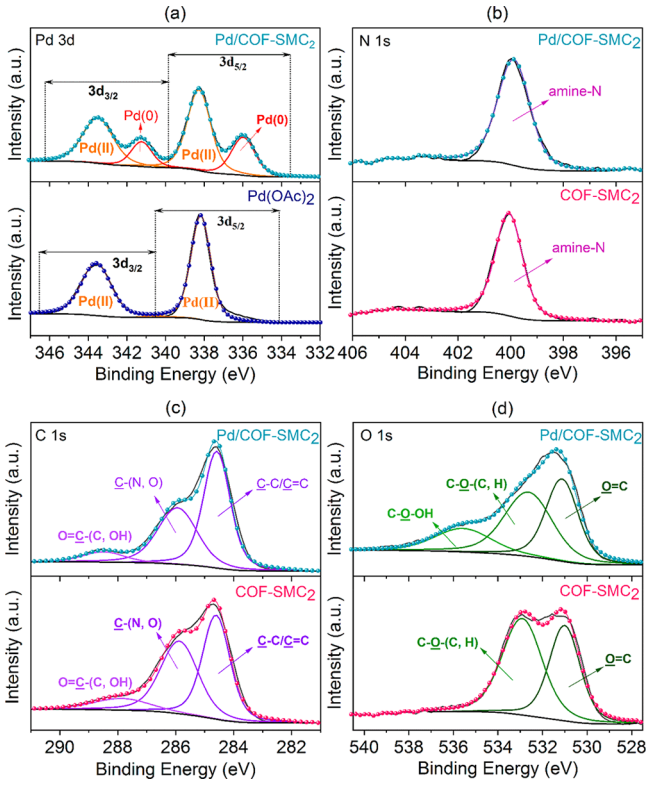


**Figure 2.** XPS spectra of the target catalyst and carrier: (a) Pd 3d, (b) N 1s, (c) C 1s, (d) O 1s.

both illustrated in Figure 1. As seen in Figure 1a, the signals of Pd/COF-SMC$_2$ do not exhibit a significant change compared to those of the parent of COF-SMC$_2$. This phenomenon indicates that Pd salt would not be an obstacle to the overall crystallinity and the host framework integrity of Pd/COF-SMC$_2$. The main peaks in the PXRD patterns at 4.72° and 7.95° were originally derived from COF-SMC$_2$, attributed to the (100) and (200) facets, respectively. The wide signal at approximate 26.7° corresponds well to the (002) reflection, which would be attributed to the $\pi-\pi$ stacking interaction between two adjacent


https://doi.org/10.1021/acsanm.1c01038
ACS Appl. Nano Mater. 2021, 4, 6239−6249

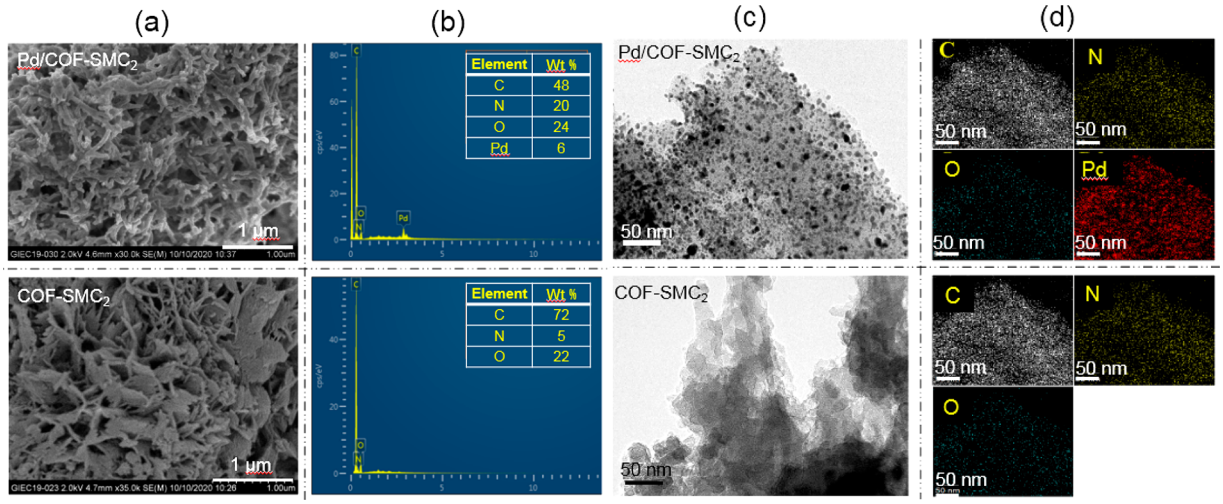


**Figure 3.** (a and b) SEM-EDS and (c and d) TEM-EDS analyzes of the target catalyst and carrier.

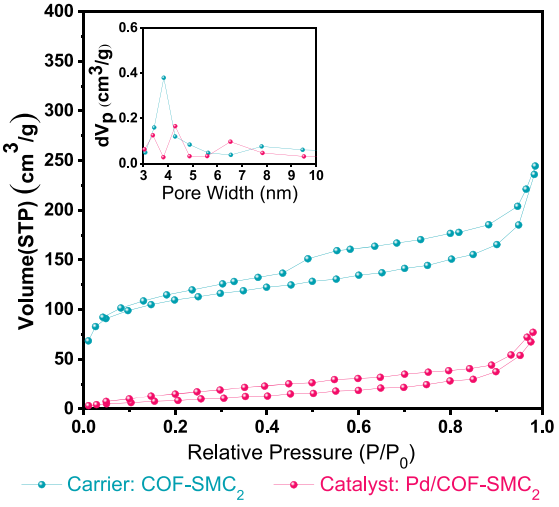


**Figure 4.** Nitrogen adsorption−desorption isotherms of the target catalyst and carrier.

layers in the COF sheets.[39] In the FTIR spectra (Figure 1b), there are intense typical absorption peaks of N—H stretching (816 $cm^{-1}$), C═O stretching (1620 $cm^{-1}$), C—N stretching (1277 $cm^{-1}$), C—H/C—O deformation (1440 $cm^{-1}$), and aryl ring stretching (1582 $cm^{-1}$), respectively,[40] suggesting the enol-keto tautomerism feature of the Pd/COF-$SMC_2$ catalyst. This can also be similarly observed in the COF-$SMC_2$ carrier material.

To confirm the chemical structure of COF-supported heterogeneous catalysts, the XPS spectra of the target catalyst and carrier were performed and are accurately fitted in Figure 2. As for Pd/COF-$SMC_2$, the target elements including C, N, O, and Pd were all discovered, matching well with the energy dispersive spectroscopy (EDS) mapping analysis results (Figure 3). The N 1s spectra can be deconvoluted into a single sharp peak at 399.9−400.1 eV for both Pd/COF-$SMC_2$ and COF-$SMC_2$, which corresponds well with the imine structure in the COF material.[41] Besides, a small shift in the binding energy of the N 1s peak was also observed between the catalyst (399.88 eV) and the carrier (400.06 eV) due to the strong Pd−N interaction,[42] suggesting the successful loading of active Pd species on the COF matrix. Moreover, in the Pd 3d spectra of free $Pd(OAc)_2$ (Figure 2a), it can be seen that the Pd (II) species presents two typical peaks (Pd $3d_{5/2}$ and Pd $3d_{3/2}$) at the binding energies of 338.2 and 343.6 eV, respectively. By comparison, it is interesting to note that the extra smaller peak (336.0 eV for Pd $3d_{5/2}$, 341.2 eV for Pd $3d_{3/2}$) was observed besides the main peak o the f Pd (II) form of Pd/COF-$SMC_2$ spectrum under two Pd 3d states, which is unequivocally assigned to metallic Pd-like species (Pd (0)).[43−46] This phenomenon would be explained by the imine groups contained in the COF structure that can donate electrons to Pd (II) species during its incorporation process, leading to the Pd species being less electron-deficient like Pd (0).[35] Hence, the resultant XPS information demonstrates that the Pd species can be coordinatively bonded to two imine nitrogen atoms from adjacent COF layers, achieving a precise regulation effect of the COF structure on Pd species by inhibiting the intrinsic activity of Pd active sites. In addition, the observed carbon-related and oxygen-related structures in Figure 2c,d are also in accordance with the functional groups in the target catalyst and carrier. The difference in the peak area of each structure is due to the extra introduction of acetate ions. Meanwhile, according to the XPS information on other comparative catalysts and carriers (Figure S2), some evidence on the detailed structure of Pd/COF-$SMC_x$ can be also provided: (1) For N 1s spectra, the only amine-N peak is found in both Pd/COF-$SMC_3$ and Pd/COF-$SMC_4$ similar to Pd/COF-$SMC_2$, whereas there is another pyridinic-N peak besides amine-N in Pd/COF-$SMC_1$. This further validates the nitrogen functionalities in each COF matrix. (2) For the Pd 3d spectra, apart from Pd/COF-$SMC_4$, other catalysts all have a certain amount of Pd (0) species with the sequence of Pd/COF-$SMC_2$ > Pd/COF-$SMC_3$ > Pd/COF-$SMC_1$. This reveals that the synthetic methods for Pd/COF-$SMC_x$ exhibit distinctive capabilities in coordinating the Pd species with the COF structure.

The morphologies of Pd/COF-$SMC_2$ and COF-$SMC_2$ were examined by SEM and TEM, as shown in Figure 3. The target catalyst and carrier both exhibit a coralline-like stacking structure linked with sticks (Figure 3a). The EDS mapping results provide evidence on the presence of target elements (C, H, O, and Pd) in the catalyst and carrier (Figure 3b). Besides, comparing the TEM images, it was seen that the Pd species were uniformly dispersed in the COFs matrix with an average particle size of 5 nm (black dots in Figure 3c). Additionally, thte EDS mapping images also illustrate the elements contained in Pd/


https://doi.org/10.1021/acsanm.1c01038
ACS Appl. Nano Mater. 2021, 4, 6239−6249

**Table 2. Catalytic Activity Test of Pd/COF-SMC$_2$ in the SMC Reaction of Phenylboronic Acid with Different Aryl Halides**

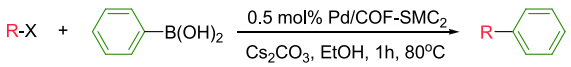


| Entry[a] | R-X | Product | Yield(%)[b] |
|---|---|---|---|
| 1 |  | 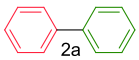 2a | 96 |
| 2 | 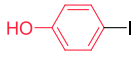 | 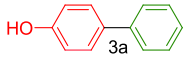 3a | 91 |
| 3 | 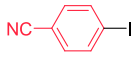 | 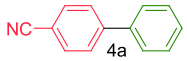 4a | 95 |
| 4 |  | 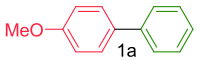 1a | 98 |
| 5 | 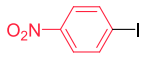 | 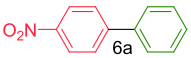 6a | 85 |
| 6 |  | 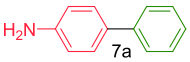 7a | 89 |
| 7 | 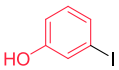 | 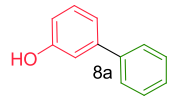 8a | 98 |
| 8 | 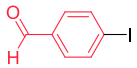 | 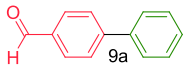 9a | 98 |
| 9 | 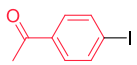 | 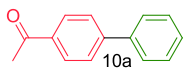 10a | 98 |
| 10 | 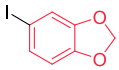 | 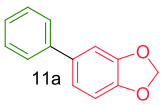 11a | 87 |
| 11 | 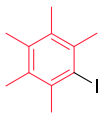 | 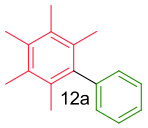 12a | 73 |
| 12 | 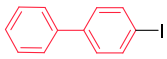 | 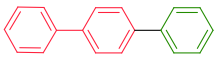 13a | 88 |
| 13 | 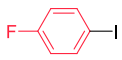 | 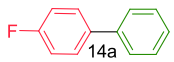 14a | 96 |
| 14 | 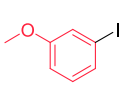 | 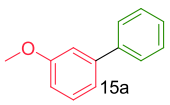 15a | 95 |
| 15 |  | 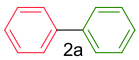 2a | 96 |

[a]Unless otherwise stated, the reaction conditions are 0.50 mmol of aryl halide, 0.75 mmol of phenylboronic acid, 1.00 mmol of $Cs_2CO_3$, 0.5 mol % of Pd/COF-SMC$_2$, 4 mL of EtOH, 1 h, 80 °C. [b]Determined by $^1$H NMR spectroscopy, based on aryl halide.

**Table 3. Catalytic Activity Test of Pd/COF-SMC$_2$ in the SMC Reaction of 1-Iodo-4-methoxybenzene with Different Aryl Boronic Acids**

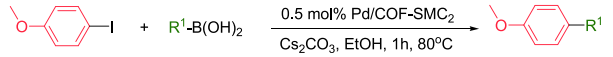


| Entry[a] | $R^1$-B(OH)$_2$ | Product | Yield(%)[b] |
|---|---|---|---|
| 1 | 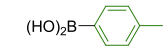 | 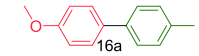 16a | 96 |
| 2 | 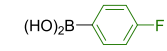 | 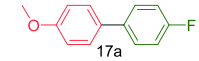 17a | 95 |
| 3 | 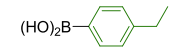 | 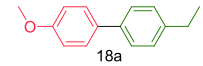 18a | 96 |
| 4 | 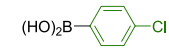 | 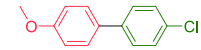 19a | 98 |
| 5 |  |  20a | 96 |
| 6 |  |  21a | 98 |
| 7 |  |  22a | 98 |
| 8 |  |  23a | 98 |
| 9 |  |  24a | 98 |
| 10 |  |  25a | 95 |
| 11 |  |  26a | 98 |
| 12 |  |  27a | 96 |
| 13 |  |  28a | 74 |
| 14 |  |  29a | 97 |
| 15 |  |  30a | 96 |
| 16 |  |  31a | 96 |

[a]Unless otherwise stated, the reaction conditions are 0.50 mmol of 1-iodo-4-methoxybenzene, 0.75 mmol of aryl boronic acid, 1.00 mmol of $Cs_2CO_3$, 0.5 mol % of Pd/COF-SMC$_2$, 4 mL of EtOH, 1 h, 80 °C. [b]Determined by $^1$H NMR spectroscopy, based on aryl halide.

COF-SMC$_2$ (Figure 3d). The Pd element was detected as well as C, N, and O, further supporting the fact of the uniform incorporation of Pd species into the COF material.

The surface area and porosity of the target catalyst and carrier were determined by nitrogen adsorption−desorption analysis (Figure 4). The Brunauer−Emmett−Teller surface areas of COF-SMC$_2$ and Pd/COF-SMC$_2$ were calculated to be 363.44 and 23.73 $m^2 \cdot g^{-1}$, respectively. On the basis of the quenched solid density functional theory (QSDFT) model, it is evident that the pore-size distribution of both COF-SMC$_2$ and Pd/COF-SMC$_2$ materials exhibits main peaks with an approximate range of 3−5 nm. Compared to the carrier COF-SMC$_2$, the catalyst Pd/COF-SMC$_2$ has a slight change in pore-size distribution with a huge decrease in surface area, demonstrating that the introduction of Pd(OAc)$_2$ would not hinder the cavities of the COF material despite the significant enhancement of its weight. The characteristics of specific surface area and regular microporous structure would make the Pd/COF-SMC$_x$ material to be a fascinating candidate in potential catalysis applications.

Pd-catalyzed cross-coupling reaction has become a widely used method for the synthesis of carbon−carbon bond formation. Particularly, it was well-recognized by the 2010 Nobel Prize that Pd-catalyzed Heck, Negishi, and Suzuki−



https://doi.org/10.1021/acsanm.1c01038
ACS Appl. Nano Mater. 2021, 4, 6239−6249

**Table 4. Catalytic Activity Test of Pd/COF-SMC$_2$ in the SMC Reaction of Functionlazide-iodo-4-methoxybenzene with Aryl Boronic Acids**[a]

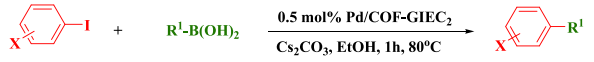


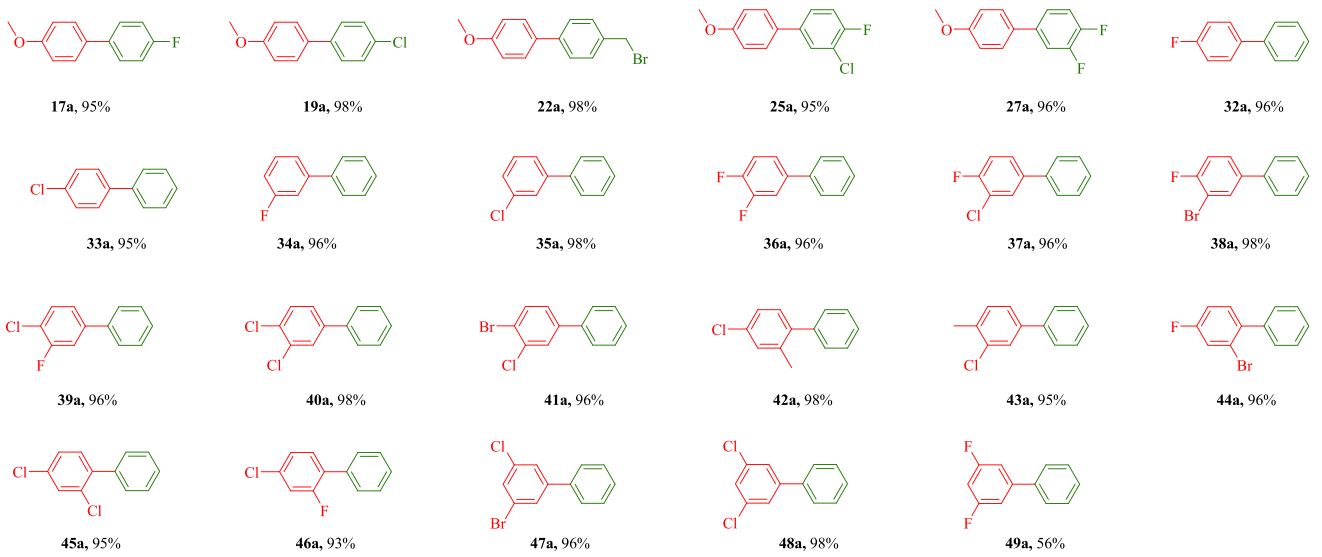


[a]Unless otherwise stated, the reaction conditions are 0.50 mmol of functionlazide-iodo-4-methoxybenzene, 0.75 mmol of aryl boronic acids, 1.00 mmol of $Cs_2CO_3$, 0.5 mol % of Pd/COF-SMC$_2$, 4 mL of EtOH, 1 h, 80 °C. [b]Determined by $^1$H NMR spectroscopy, based on aryl halide.

Miyaura couplings are considered essential. There are some disadvantages like toxicity, difficult separation, and hard recyclability of the homogeneous catalyst Pd, which limit the potential application in the industry. Pd-based heterogeneous catalyst, in this context, is preferred predominately for industrial production since it is easier to be separated and recycled, reducing operating costs and avoiding unwanted traces of toxic metals in the final products.

With the confirmation of the optimal reaction conditions, the scope of SMC reaction of phenylboronic acid with different aryl halides was subsequently investigated. As shown in Table 2, under the catalytic effect of Pd/COF-SMC$_2$, most of aryl halides substrates would be directionally converted to the biaryl products with high yield (up to 98%), demonstrating the advantage of this catalyst in the application area with heterogeneous SMC reaction. Furthermore, the sterically hindered substrate can be also converted successfully to the corresponding biaryl product **12a** (entry 11) in good yield.

Next, we assessed the catalytic capacity of Pd/COF-SMC$_2$ on the SMC reaction of 1-iodo-4-methoxybenzene with different aryl boronic acids (Table 3). A series of boronic acid derivative substrates with varying functional groups at the *para*-, *meta*-, and *para*, *meta*-positions were evaluated under optimal reaction conditions. As presented in Table 3, the majority of these substrates would be high-efficiently converted with the help of Pd/COF-SMC$_2$, and the target biaryl products with very high yields were obtained (15 examples). Due to the halogenated boronic acid self-coupling reaction and low yield of the target SMC reaction product, the halogenated aryl boronic acid substrates have been seldom reported previously. To our excitement, many target halo-substituted biaryl products **17a** (entry 2), **19a** (entry 4), **22a** (entry 7), **25a** (entry 10), and **27a** (entry 12) were obtained with excellent yields after 1 h at a 80 °C reaction. The substrates with different *para*-substituted multi-functional groups such as alkyl, ether, cyano, ketone, and ester were well-tolerated and showed good yields for the desired products.

Halo-substituted aryl, biaryl compounds are very useful and widely used in coupling reactions, total synthesis, and materials synthesis as well as in industry and academia. As shown in Table 4, the heterogeneous COF-supported catalyst Pd/COF-SMC$_2$ can high-selectively recognize between I- and Br-functional groups in the same reagent (**22a**, **38a**, **41a**, **44a**, and **47a**). More than 20 halo-substituted biaryl products were gained in good yields under the standard reaction conditions. Further investigation of the stability of the Pd/COF-SMC$_2$ catalyst in the SMC reaction showed that this catalyst could be reused three times without losing significant activity.

Using the Pd/COF catalysts, the SMC reaction acts as heterogeneous catalysis. During the reaction process, Pd (II) could be released from the surface of the COF support ligand and the leaching Pd could be responsible for the catalysis as a (quasi)homogeneous mechanism, as shown in Scheme 3.[47−49] In the oxidative addition step, 1-iodo-4-methoxybenzene (MeOPh-I) diffuses through the microporous structure of COF support and then reaches the active sites of the Pd nanoparticle. Then, the Pd leaching phenomenon stems from the oxidative reaction between the inner Pd/COF catalyst and the infiltrating MeOPh-I, transforming Pd (0) into Pd (II) and leading to the formation of surface intermediate MeOPh-Pd-I. This intermediate (MeOPh-Pd-I) can desorb and then transfer across the porous COF support, joining in the reaction solution system. Then, the *trans*-metalation of MeOPh-Pd-I and aryl boronic acid would happen inevitably, leading to the formation of biaryl palladium type MeOPh-Pd(II)-Ph. Finally, the biaryl product MeOPh-Ph can be formed via the reductive elimination of Pd from the MeOPh-Pd(II)-Ph intermediate. Simultaneously, the Pd (II) state will be reduced into Pd (0) state.



https://doi.org/10.1021/acsanm.1c01038
ACS Appl. Nano Mater. 2021, 4, 6239−6249

**Scheme 3. Mechanism for Pd/COF-Catalyzed Suzuki−Miyaura Cross-Coupling Reactions**

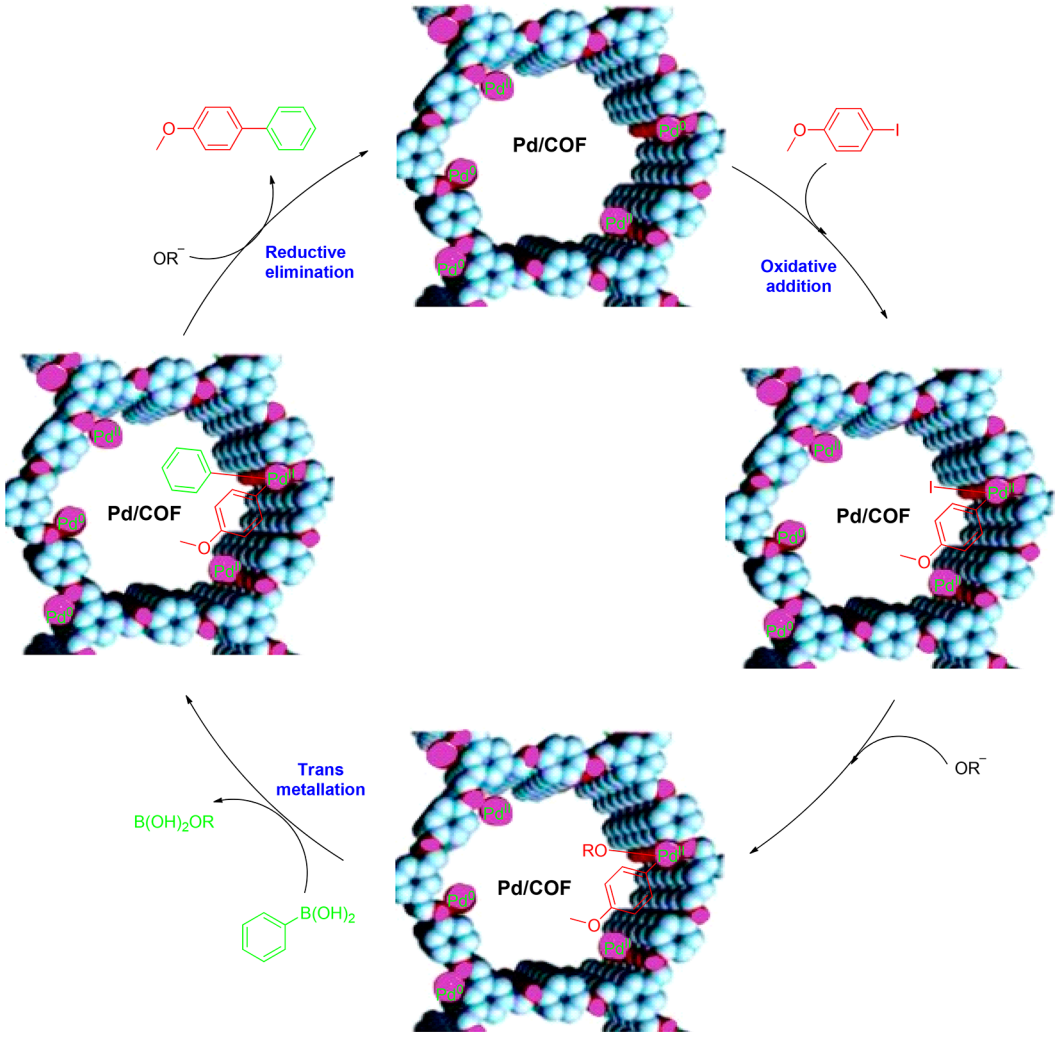


## CONCLUSION

In summary, we have successfully designed and prepared a series of COF-SMC carrier materials using a simple feasible solvothermal method in an environmentally-friendly way. We also developed the first precise control activity of the Pd/COF-SMC nanoparticles catalyst for the establishment of C—C bonds via region-selective Suzuki−Miyaura cross-coupling of aryl boronic acids and aryl halides, especially with halogenated aryl boronic acids. Under the cooperative catalysis of nanoparticles Pd/COF-SMC with $Cs_2CO_3$, we undertook the synthesis of >40 biaryl products and more than 20 halo-substituted biaryl products in excellent yield. The methodology is moderate, tolerant to functional groups, friendly to the environment, and has an outstanding advantage of precise regulation nanoparticles Pd properties activity, which can be strategically applied in varying transition metal-catalyzed cross-coupling series to build with or without halo-substituted moiety.

## ASSOCIATED CONTENT

### Supporting Information

The Supporting Information is available free of charge at https://pubs.acs.org/doi/10.1021/acsanm.1c01038.

Discussions of general methods, synthetic methods, and general procedure of Suzuki−Miyaura cross-coupling (SMC) reaction, figures of PXRD patterns, FTIR spectra, XPS spectra, SEM-EDS information, nitrogen adsorption−desorption isotherms, pore-size distribution, TEM images, and NMR spectra, table of specific surface area, pore volume, pore diameter, yield, and Pd loading of Pd/COF-SMC$_x$, and schemes of distinctive mechanisms of Pd-catalyzed SMC reactions and typical Pd-catalyzed SMC reactions (PDF)

## AUTHOR INFORMATION

### Corresponding Authors

**Jianguo Liu** − *Key Laboratory of Renewable Energy, CAS, Guangdong Key Laboratory of New and Renewable Energy Research and Development, Guangzhou Institute of Energy Conversion, Chinese Academy of Sciences, Guangzhou 510640, China;* orcid.org/0000-0001-5105-5114; Email: Liujg@ms.giec.ac.cn

**Longlong Ma** − *Key Laboratory of Renewable Energy, CAS, Guangdong Key Laboratory of New and Renewable Energy Research and Development, Guangzhou Institute of Energy Conversion, Chinese Academy of Sciences, Guangzhou 510640, China; School of Environmental Science and Engineering, Tianjin University, Tianjin 300350, China;* orcid.org/0000-0003-3848-5149; Email: Mall@ms.giec.ac.cn



https://doi.org/10.1021/acsanm.1c01038
ACS Appl. Nano Mater. 2021, 4, 6239−6249

### Authors

**Hao Zhan** − *State Key Laboratory of Organic Geochemistry, Guangdong Key Laboratory of Environmental Protection and Resources Utilization, Guangzhou Institute of Geochemistry, Chinese Academy of Sciences, Guangzhou 510640, China*

**Nan Wang** − *School of Environmental Science and Engineering, Tianjin University, Tianjin 300350, China*

**Yanpei Song** − *Key Laboratory of Renewable Energy, CAS, Guangdong Key Laboratory of New and Renewable Energy Research and Development, Guangzhou Institute of Energy Conversion, Chinese Academy of Sciences, Guangzhou 510640, China*

**Chenguang Wang** − *Key Laboratory of Renewable Energy, CAS, Guangdong Key Laboratory of New and Renewable Energy Research and Development, Guangzhou Institute of Energy Conversion, Chinese Academy of Sciences, Guangzhou 510640, China;* orcid.org/0000-0002-1950-006X

**Xinming Wang** − *State Key Laboratory of Organic Geochemistry, Guangdong Key Laboratory of Environmental Protection and Resources Utilization, Guangzhou Institute of Geochemistry, Chinese Academy of Sciences, Guangzhou 510640, China;* orcid.org/0000-0002-1982-0928

**Lungang Chen** − *Key Laboratory of Renewable Energy, CAS, Guangdong Key Laboratory of New and Renewable Energy Research and Development, Guangzhou Institute of Energy Conversion, Chinese Academy of Sciences, Guangzhou 510640, China*

Complete contact information is available at: https://pubs.acs.org/10.1021/acsanm.1c01038


### Author Contributions

[‖]J.L., H.Z., and N.W. contributed equally to this work. L.M. and J.L. supervised and designed the research. J.L., N.W., and H.Z. performed most of the experiments and data analysis. Y.S. helped catalysts characterization. X.W. and C.W. performed useful discussion and data analysis. J.L. and H.Z. cowrote the paper. All authors discussed the results and assisted the manuscript preparation.

### Notes

The authors declare no competing financial interest.

## ■ ACKNOWLEDGMENTS

This work was supported financially by the National Key R&D Program of China (2019YFD1100601), National Natural Science Foundation of China (51976225), and DNL Cooperation Fund, CAS (DNL201916).

## ■ REFERENCES


(1) Corbet, J. P.; Mignani, G. Selected patented cross-coupling reaction technologies. *Chem. Rev.* **2006**, *106*, 2651−2710.

(2) Seechurn, C. C. C. J.; Kitching, M. O.; Colacot, T. J.; Snieckus, V. Palladium-catalyzed cross-coupling: A historical contextual perspective to the 2010 Nobel Prize. *Angew. Chem., Int. Ed.* **2012**, *51*, 5062−5085.

(3) Thomas, A. A.; Denmark, S. E. Pre-transmetalation intermediates in the Suzuki-Miyaura reaction revealed: The missing link. *Science* **2016**, *352*, 329−332.

(4) Handa, S.; Wang, Y.; Gallou, F.; Lipshutz, B. H. Sustainable Fe-ppm Pd nanoparticle catalysis of Suzuki-Miyaura cross-couplings in water. *Science* **2015**, *349*, 1087−1091.

(5) Weires, N. A.; Baker, E. L.; Garg, N. K. Nickel-catalysed Suzuki-Miyaura coupling of amides. *Nat. Chem.* **2016**, *8*, 75−79.

(6) Malapit, C. A.; Bour, J. R.; Brigham, C. E.; Sanford, M. S. Base-free nickel-catalysed decarbonylative Suzuki-Miyaura coupling of acid fluorides. *Nature* **2018**, *563*, 100−104.

(7) Martin, R.; Buchwald, S. L. Palladium-catalyzed Suzuki-Miyaura cross-coupling reactions employing dialkylbiaryl phosphine ligands. *Acc. Chem. Res.* **2008**, *41*, 1461−1473.

(8) Miyaura, N.; Yamada, K.; Suzuki, A. New stereospecific cross-coupling by the palladium-catalyzed reaction of 1-alkenylboranes with 1-alkenyl or 1-alkynyl halides. *Tetrahedron Lett.* **1979**, *20*, 3437−3440.

(9) Wong, S. M.; So, C. M.; Chung, K. H.; Luk, C. H.; Lau, C. P.; Kwong, F. Y. P, N-Type benzimidazolyl phosphine ligands for the palladium-catalyzed Suzuki coupling of potassium aryltrifluoroborates and aryl chlorides. *Tetrahedron Lett.* **2012**, *53*, 3754−3757.

(10) Chow, W. K.; Yuen, O. Y.; So, C. M.; Wong, W. T.; Kwong, F. Y. Carbon-boron bond cross-coupling reaction catalyzed by -$PPh_2$ containing palladium-indolylphosphine complexes. *J. Org. Chem.* **2012**, *77*, 3543−3548.

(11) Marion, N.; Navarro, O.; Mei, J.; Stevens, E. D.; Scott, N. M.; Nolan, S. P. Modified (NHC)Pd(allyl)Cl (NHC = N-Heterocyclic Carbene) complexes for room-temperature Suzuk-Miyaura and Buchwald-Hartwig reactions. *J. Am. Chem. Soc.* **2006**, *128*, 4101−4111.

(12) Das, P.; Sarmah, C.; Tairai, A.; Bora, U. Highly efficient amine-based catalytic system for room temperature Suzuki-Miyaura reactions of aryl halides with arylboronic acids. *Appl. Organomet. Chem.* **2011**, *25*, 283−288.

(13) Susanto, W.; Chu, C.-Y.; Ang, W. J.; Chou, T.-C.; Lo, L.-C.; Lam, Y. Development of a fluorous, oxime-based palladacycle for microwave-promoted carbon-carbon coupling reactions in aqueous media. *Green Chem.* **2012**, *14*, 77−80.

(14) Dewan, A.; Bora, U.; Borah, G. A simple and efficient tetradentate Schiff base derived palladium complex for Suzuki-Miyaura reaction in water. *Tetrahedron Lett.* **2014**, *55*, 1689−1692.

(15) Lee, D. H.; Jung, J. Y.; Jin, M. J. Highly active and recyclable silica gel-supported palladium catalyst for mild cross-coupling reactions of unactivated heteroaryl chlorides. *Green Chem.* **2010**, *12*, 2024−2029.

(16) Kumbhar, A. Palladium catalyst supported on zeolite for cross-coupling reactions: An overview of recent advances. *Topics Curr. Chem.* **2017**, *375*, 2.

(17) Sun, J.; Fu, Y.; He, G.; Sun, X.; Wang, X. Green Suzuki-Miyaura coupling reaction catalyzed by palladium nanoparticles supported on graphitic carbon nitride. *Appl. Catal., B* **2015**, *165*, 661−667.

(18) Gulcan, M.; Zahmakiran, M.; Ozkar, S. Palladium(0) nanoparticles supported on metal organic framework as highly active and reusable nanocatalyst in dehydrogenation of dimethylamine-borane. *Appl. Catal., B* **2014**, *147*, 394−401.

(19) Shen, Y.; Tong, Y.; Xu, J.; Wang, S.; Wang, J.; Zeng, T.; He, Z.; Yang, W.; Song, S. Ni-based layered metal-organic frameworks with palladium for electrochemical dechlorination. *Appl. Catal., B* **2020**, *264*, 118505.

(20) Tanaka, S.; Kaneko, T.; Asao, N.; Yamamoto, Y.; Chen, M.; Zhang, W.; Inoue, A. A nanostructured skeleton catalyst: Suzuki-coupling with a reusable and sustainable nanoporous metallic glass Pd-catalyst. *Chem. Commun.* **2011**, *47*, 5985−5987.

(21) Paul, S.; Islam, M. M.; Islam, S. M. Suzuki-Miyaura reaction by heterogeneously supported Pd in water: recent studies. *RSC Adv.* **2015**, *5*, 42193−42221.

(22) Bedford, R. B.; Cazin, C. S. J.; Holder, D. The development of palladium catalysts for CC and Cheteroatom bond forming reactions of aryl chloride substrates. *Coord. Chem. Rev.* **2004**, *248*, 2283−2321.

(23) Wang, B.; Yue, Y.; Jin, C.; Lu, J.; Wang, S.; Yu, L.; Guo, L.; Li, R.; Hu, Z.-T.; Pan, Z.; Zhao, J.; Li, X. Hydrochlorination of Acetylene on Single-Atom Pd/N-Doped Carbon Catalysts: Importance of Pyridinic-N Synergism. *Appl. Catal., B* **2020**, *272*, 118944.

(24) Álvarez-Casao, Y.; Monge, D.; Álvarez, E.; Fernández, R.; Lassaletta, J. M. Pyridine-hydrazones as N, N′-Ligands in asymmetric catalysis: Pd(II)-catalyzed addition of boronic acids to cyclic sulfonylketimines. *Org. Lett.* **2015**, *17*, 5104−5107.

(25) Cote, A. P.; Benin, A. I.; Ockwig, N. W.; O'Keeffe, M.; Matzger, A. J.; Yaghi, O. M. Porous, crystalline, covalent organic frameworks. *Science* **2005**, *310*, 1166−1170.

(26) Bunck, D. N.; Dichtel, W. R. Internal functionalization of three-dimensional covalent organic frameworks. *Angew. Chem., Int. Ed.* **2012**, *51*, 1885−1889.
(27) Kandambeth, S.; Mallick, A.; Lukose, B.; Mane, M. V.; Heine, T.; Banerjee, R. Construction of crystalline 2D covalent organic frameworks with remarkable chemical (acid/base) stability via a combined reversible and irreversible route. *J. Am. Chem. Soc.* **2012**, *134*, 19524−19527.
(28) Furukawa, H.; Yaghi, O. M. Storage of hydrogen, methane, and carbon dioxide in highly porous covalent organic frameworks for clean energy applications. *J. Am. Chem. Soc.* **2009**, *131*, 8875−8883.
(29) Tong, M. M.; Yang, Q. Y.; Zhong, C. L. Computational screening of covalent organic frameworks for $CH_4/H_2$, $CO_2/H_2$ and $CO_2/CH_4$ separations. *Microporous Mesoporous Mater.* **2015**, *210*, 142−148.
(30) Tong, M. M.; Yang, Q. Y.; Xiao, Y. L.; Zhong, C. L. Revealing the structure-property relationship of covalent organic frameworks for $CO_2$ capture from postcombustion gas: a multi-scale computational study. *Phys. Chem. Chem. Phys.* **2014**, *16*, 15189−15198.
(31) Chen, L.; Furukawa, K.; Gao, J.; Nagai, A.; Nakamura, T.; Dong, Y.; Jiang, D. Photoelectric covalent organic frameworks: converting open lattices into ordered donor-acceptor heterojunctions. *J. Am. Chem. Soc.* **2014**, *136*, 9806−9809.
(32) Yang, Q.; Luo, M.; Liu, K.; Cao, H.; Yan, H. Covalent organic frameworks for photocatalytic applications. *Appl. Catal., B* **2020**, *276*, 119174.
(33) Xu, Y.; Shi, X.; Hua, R.; Zhang, R.; Yao, Y.; Zhao, B.; Liu, T.; Zheng, J.; Lu, G. Remarkably catalytic activity in reduction of 4-nitrophenol and methylene blue by $Fe_3O_4$@COF supported noble metal nanoparticles. *Appl. Catal., B* **2020**, *260*, 118142.
(34) Pachfule, P.; Acharjya, A.; Roeser, J.; Langenhahn, T.; Schwarze, M.; Schomäcker, R.; Thomas, A.; Schmidt, J. Diacetylene functionalized covalent organic framework (COF) for photocatalytic hydrogen generation. *J. Am. Chem. Soc.* **2018**, *140*, 1423−1427.
(35) Ding, S.-Y.; Gao, J.; Wang, Q.; Zhang, Y.; Song, W.-G.; Su, C.-Y.; Wang, W. Construction of covalent organic framework for catalysis: Pd/COF-LZU1 in Suzuki-Miyaura coupling reaction. *J. Am. Chem. Soc.* **2011**, *133*, 19816−19822.
(36) Huang, N.; Wang, P.; Jiang, D. Covalent organic frameworks: a materials platform for structural and functional designs. *Nat. Rev. Mater.* **2016**, *1*, 16068.
(37) Hou, Y.; Zhang, X.; Sun, J.; Lin, S.; Qi, D.; Hong, R.; Li, D.; Xiao, X.; Jiang, J. Good Suzuki-coupling reaction performance of Pd immobilized at the metal-free porphyrin-based covalent organic framework. *Microporous Mesoporous Mater.* **2015**, *214*, 108−114.
(38) Goncalves, R. S. B.; de Oliveira, A. B. V.; Sindra, H. C.; Archanjo, B. S.; Mendoza, M. E.; Carneiro, L. S. A.; Buarque, C. D.; Esteves, P. M. Heterogeneous catalysis by covalent organic frameworks (COF): $Pd(OAc)_2$@COF-300 in cross-coupling reactions. *ChemCatChem* **2016**, *8*, 743−750.
(39) Bhadra, M.; Sasmal, H. S.; Basu, A.; Midya, S. P.; Kandambeth, S.; Pachfule, P.; Balaraman, E.; Banerjee, R. Predesigned metal-anchored building block for in situ generation of Pd nanoparticles in porous covalent organic framework: application in heterogeneous tandem catalysis. *ACS Appl. Mater. Interfaces* **2017**, *9*, 13785−13792.
(40) Chen, R.; Shi, J.-L.; Ma, Y.; Lin, G.; Lang, X.; Wang, C. Designed synthesis of a 2D porphyrin-based $sp^2$ Carbon-conjugated covalent organic framework for heterogeneous photocatalysis. *Angew. Chem., Int. Ed.* **2019**, *58*, 6430−6434.
(41) Sun, Q.; Aguila, B.; Ma, S. Q. A bifunctional covalent organic framework as an efficient platform for cascade catalysis. *Mater. Chem. Front.* **2017**, *1*, 1310−1316.
(42) Wojcieszak, R.; Genet, M. J.; Eloy, P.; Ruiz, P.; Gaigneaux, E. M. Determination of the size of supported Pd nanoparticles by X-ray photoelectron spectroscopy. comparison with X-ray diffraction, transmission electron microscopy, and $H_2$ chemisorption methods. *J. Phys. Chem. C* **2010**, *114*, 16677−16684.
(43) Dumbuya, K.; Denecke, R.; Steinruck, H. P. Surface analysis of Pd/ZnO catalysts dispersed on micro-channeled Al-foils by XPS. *Appl. Catal., A* **2008**, *348*, 209−213.
(44) Bayer, A.; Flechtner, K.; Denecke, R.; Steinrück, H.-P.; Neyman, K. M.; Rösch, N. Electronic properties of thin Zn layers on Pd(III) during growth and alloying. *Surf. Sci.* **2006**, *600*, 78−94.
(45) Brun, M.; Berthet, A.; Bertolini, J. C. XPS, AES and Auger parameter of Pd and PdO. *J. Electron Spectrosc. Relat. Phenom.* **1999**, *104*, 55−60.
(46) Taylor, R. H.; Felpin, F. X. Suzuki-Miyaura reactions of arenediazonium salts catalyzed by Pd(0)/C. one-pot chemoselective double cross-coupling reactions. *Org. Lett.* **2007**, *9*, 2911−2914.
(47) Cantillo, D.; Kappe, C. O. Immobilized Transition Metals as Catalysts for Cross-Couplings in Continuous Flow-A Critical Assessment of the Reaction Mechanism and Metal Leaching. *ChemCatChem* **2014**, *6*, 3286−3305.
(48) Thathagar, M. B.; Ten Elshof, J. E.; Rothenberg, G. Pd nanoclusters in C-C coupling reactions: Proof of leaching. *Angew. Chem., Int. Ed.* **2006**, *45*, 2886−2890.
(49) Reetz, M. T.; Westermann, E. Phosphane-free palladium-catalyzed coupling reactions: The decisive role of Pd nanoparticles. *Angew. Chem., Int. Ed.* **2000**, *39*, 165−168.


https://doi.org/10.1021/acsanm.1c01038
*ACS Appl. Nano Mater.* 2021, 4, 6239−6249